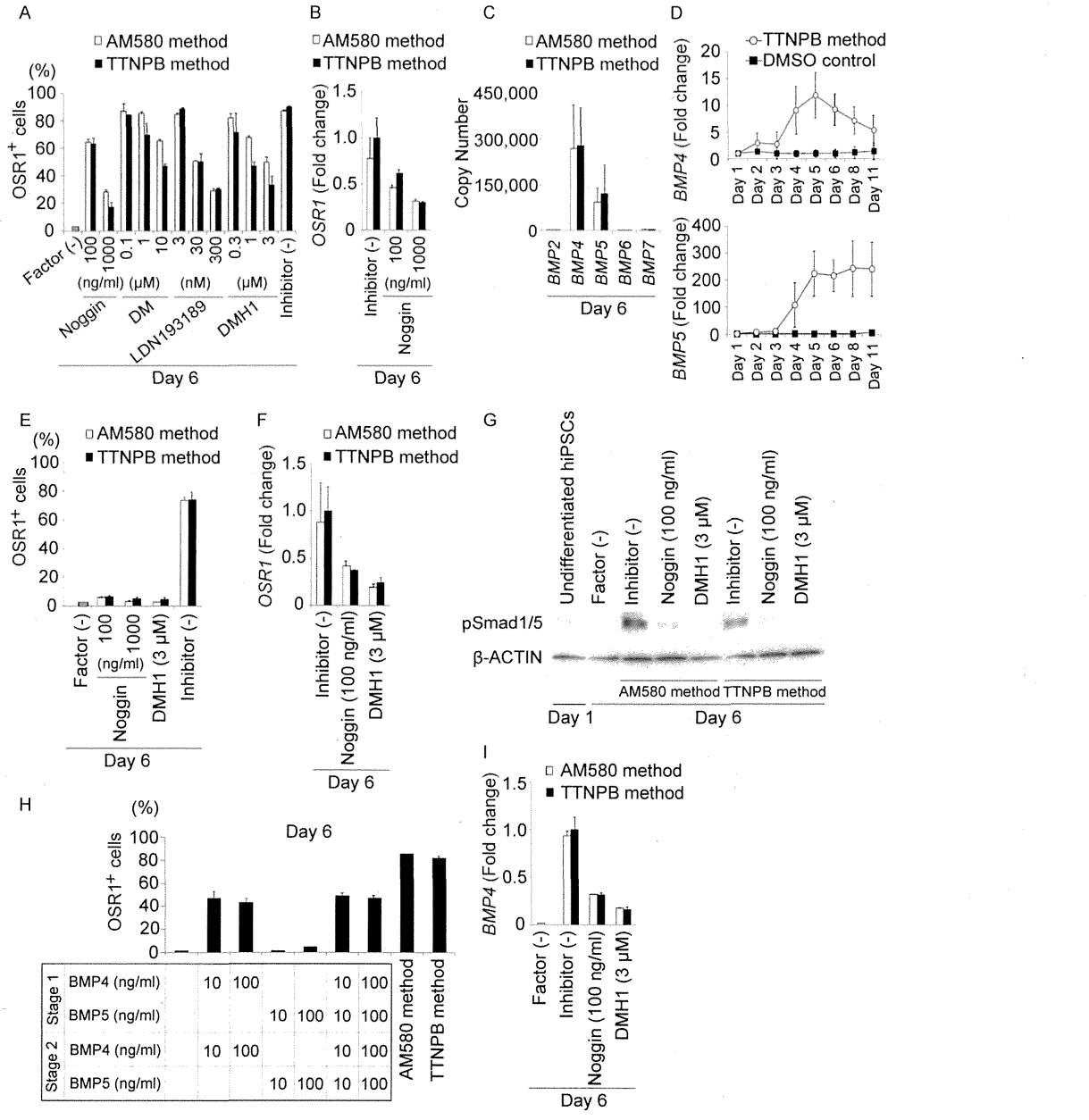

Figure 5. The BMP-Smad Signaling Pathway Regulates Development of IM. (A) Results of the flow cytometric analyses examining the effects of adding noggin, dorsomorphin (DM), LDN193189 and DMH1 during Stage 2 on the induction of OSR1$^+$ cells on culture day 6 in the AM580 and TTNPB methods. (B) Results of qRT-PCR analyses showing mRNA expression of *OSR1* on culture day 6 of the AM580 and TTNPB methods, with or without noggin. (C) Copy numbers of *BMP-2*, *-4*, *-5*, *-6*, and *-7* expressed in differentiation cultures. (D) Time course of *BMP-4* and *BMP-5* mRNA expression in the TTNPB method. OSR1-GFP knock-in hiPSCs prior to treatments were used to normalize the data. (E and F) Effects of adding noggin or DMH1 during Stages 1 and 2 on the induction of OSR1$^+$ cells and the *OSR1* expression levels analyzed on culture day 6. (G) Results of Western blot analyses examining phosphorylation levels of Smad1/5 in differentiation cultures of the small molecule method, with or without noggin or DMH1 added to Stages 1 and 2. (H) OSR1$^+$ cell induction on culture day 6 in the small molecule method and following treatment with various combinations of recombinant BMP-4 and BMP-5 proteins. (I) Results of qRT-PCR analyses showing *BMP-4* mRNA expression in differentiation cultures on day 6 of the small molecule method, with or without the addition of noggin or DMH1. Factor (-) indicates the rate of induction of OSR1$^+$ cell (A and E), the phosphorylation level of Smad1/5 (G) and the mRNA expression level of *BMP4* (I), on day 6 of the differentiation culture without growth factors or small molecules. OSR1-GFP knock-in hiPSCs obtained on day 6 following treatment of the TTNPB method without inhibitors were used to normalize the data shown in (B), (F) and (I). The data in (A–F, H, I) are means±SD of three independent experiments (n = 3). The data in (G) are representative of three independent experiments.

doi:10.1371/journal.pone.0084881.g005

To further elucidate the regulatory mechanisms involved in increasing BMP-4 expression, we used qRT-PCR analysis to examine the effects of adding noggin or DMH1 on the expression of *BMP-4*. We found that the expression levels of both *BMP-4* and *OSR1* were reduced by adding BMP inhibitors (Figures 5F and I), suggesting that expression of *BMP-4* is regulated not only by the treatment with CHIR99021 and AM580 or TTNPB, but also by BMP-4 that is secreted from the induced cells, in a positive feedback manner.

The Small Molecule Method Directly Generates IM Cells without the Mesendoderm Step

In the small molecule method, peak induction of $OSR1^+$ cells occurs around culture day 6, compared to day 10 in the growth factor method [19] (Figures 2A, B and Figure S2A). We tested the hypothesis that treatment with CHIR99021 and TTNPB generates mesendoderm cells faster than treatment with CHIR99021 and activin A by examining differentiation of $BRACHYURY^+$ mesendoderm cells after 24, 48, 72, and 96 hrs of each treatment. Surprisingly, while treatment with CHIR99021 and activin A differentiated hiPSCs into $BRACHYURY^+$ cells at an induction rate >80%, treatment with CHIR99021 and TTNPB resulted in a rate only around 6%, even at the peak time (48 hrs, Figure 6A). Then, we used qRT-PCR analyses to examine temporal expression patterns of three mesendoderm markers, *BRACHYURY*, *GOOSECOID*, and *MIXL1*, in differentiation cultures treated by the growth factor vs. TTNPB method. The expression levels induced by the TTNPB method were markedly lower than those induced by the growth factor method (Figure 6B), suggesting that the small molecule method produces IM cells without going through the mesendoderm step.

Notably, we found that the induction of $OSR1^+$ IM cells by the growth factor method was significantly reduced by the addition of the RAR inhibitor, BMS493, without a concomitant reduction of $BRACHYURY^+$ cell differentiation (Figures 6C and D). Furthermore, expression of *RARB* was detected on day 4 or later in the growth factor method (Figure 6E), which indicates that the induced RA signaling plays an essential role in IM differentiation, not only by the small molecule method but also by the growth factor method. As both CHIR99021 and BMP-7 were used during Stage 2 of the growth factor method, the combination of Wnt, RA, and BMP pathways are involved in the IM differentiation by both methods.

Overall, the results suggest that IM cells can be induced through activation of the Wnt, RA, and BMP pathways, without the mesendoderm step, and that the delay of the RA signal activation might result in the delayed generation of IM cells by the growth factor method as compared to the small molecule method.

Discussion

Regenerative medicine is associated with high costs and enormous time requirements, because generation of large numbers of targeted cell types is necessary for clinical applications, such as cell therapy, and the efficiency of cell differentiation is generally low. Therefore, rapid, efficient, and relatively low-cost methods for differentiating hiPSCs/ESCs into target cell types are highly desirable. Previous studies differentiated hiPSCs/ESCs into renal lineage cells by combined treatment with activin A, BMP, and RA, but did not report induction rates [30,31]. We recently developed a method for quantifying the induction rate of IM cells by generating a reporter hiPSC line for OSR1, and subsequently developed a differentiation method for IM cells using growth factors, with an induction rate >90% [19]. The goal of the present study was to identify small molecules that provide similarly high induction rates, but that are less expensive and more consistently effective than growth factors. We have identified two small molecules, AM580 and TTNPB, that are potent inducers of IM differentiation from hiPSCs, and developed a small molecule differentiation method, using just two chemicals, that is more rapid, more consistently effective, and less expensive than the growth factor method.

The IM cells generated using the small molecule method exhibited a developmental potential to further differentiate into cells of IM-derivative organs, such as the kidneys, adrenal cortex and genitalia both *in vitro* and *in vivo*, and form three-dimensional renal tubular structures in an organ culture setting. These findings were similarly observed in the IM cells generated using the growth factor method; however, the frequency of tubular formation in the organ culture samples was much higher in the samples obtained using the small molecule method (approximately 50%) than in those obtained using the growth factor method (approximately 5%) [19]. In addition, the small molecule method more robustly generated IM cells than the growth factor method in terms of the cell number yielded, which is advantageous for the development of regenerative medicine strategies (Figures 2B, C and Figures S2A, B, S5).

Mouse embryonic tissues at the gastrulation stage are capable of RA synthesis, which occurs preferentially in the node and primitive streak [50], suggesting that RA signaling pathways play some roles in early development. RA treatments have been used to induce pronephric tissues *in vitro* from an animal cap [23–25], and to induce renal lineage cells from mESCs [26–28] and hESCs/iPSCs [30,31]. A recent report has described the involvement of signaling through RAR, but not through RXR, in the mESC differentiation into IM cells [29]. However, the roles and mechanisms of RA signaling in the differentiation of renal lineage cells have not been fully elucidated, especially in human.

Results of the present study demonstrated that signals through RAR also play an essential role in human IM cell differentiation, that RARβ, one of the three RAR subtypes is involved in the induction process, and that one of the downstream players is the BMP-Smad1/5 pathway, which is known to regulate cell fate decisions of mesoderm tissues [32,33]. Furthermore, the BMP signaling inhibitors, noggin and DMH1, inhibited IM differentiation and *BMP-4* expression, suggesting that positive feedback mechanisms in the BMP signaling pathways are activated when IM is generated. We also showed that TTNPB and AM580 most efficiently induce IM cells among the retinoids we examined.

It has been reported that all mesoderm and endoderm tissues, including IM, are derived from a common mesendoderm precursor *in vivo* [51] and *in vitro* [52]. We first aimed to generate IM cells through the mesendoderm and confirmed that treatment with CHIR99021 alone can induce the differentiation of mesendoderm cells. However, we accidentally found that the addition of TTNPB to CHIR99021 in stage 1 blocked the differentiation of the cells into the mesendoderm. The resultant small molecule method directly induced the differentiation of IM cells without the mesendoderm step by activating the Wnt, RA and BMP signaling pathways. Furthermore, we confirmed that RA signaling plays an essential role in IM differentiation, but not mesendoderm differentiation, in the growth factor method, although the activation of the RA pathway was delayed compared to that observed in the small molecule method. Therefore, we reasoned that the generation of IM cells using the small molecule method requires less time than that performed using the growth factor method (Figure 2B and Figures S2A, S5). Our results also suggest that target cells, including IM cells, can be directly

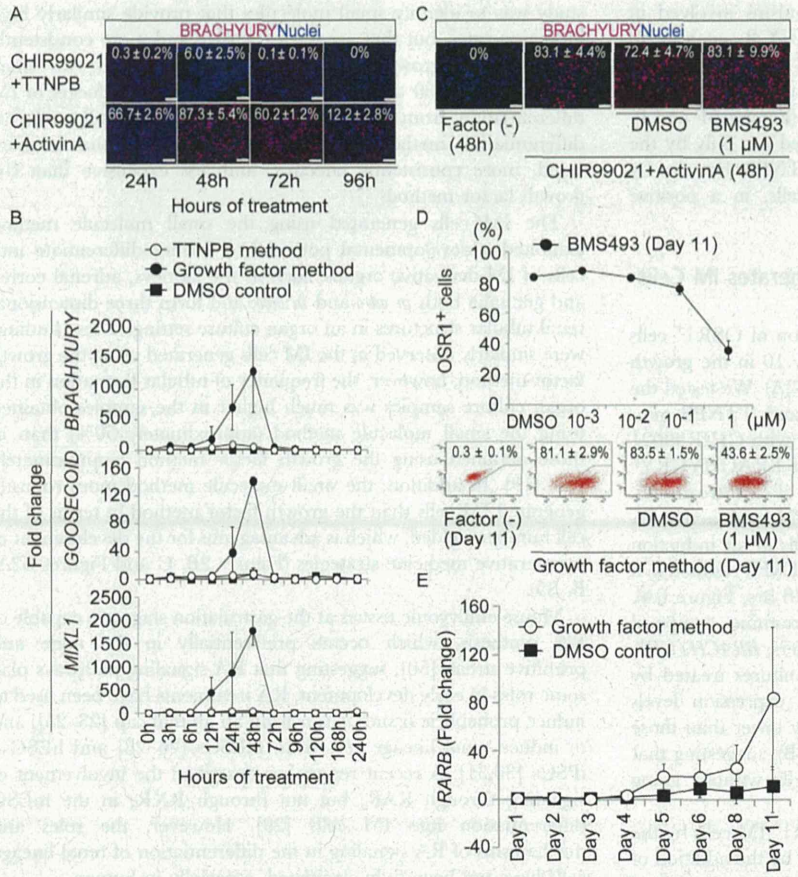

Figure 6. The Small Molecule Method Can Produce IM Cells without the Mesendoderm Step. (A) Induction of BRACHYURY$^+$ mesendoderm cells generated from OSR1-GFP knock-in hiPSCs (3D45) after 24, 48, 72, and 96 hrs of treatment with CHIR99021 and TTNPB or activin A. (B) Results of the qRT-PCR analyses showing mRNA expression of the mesendoderm markers, *BRACHYURY*, *GOOSECOID*, and *MIXL1*, in differentiation cultures from the growth factor and TTNPB methods. (C) Effects of adding a RAR inhibitor, BMS493, to differentiation cultures of 3D45 cells treated with CHIR99021 and activin A, analyzed by anti-BRACHYURY immunostaining. (D) Induction of OSR1$^+$ cells on culture day 11 of the growth factor method, with or without addition of BMS493 at various concentrations. (E) Results of qRT-PCR analyses showing expression of *RARB* mRNA. 3D45 cells on day 1, before treatment, were used to normalize the data shown in (B) and (E). The data in (A–E) are means±SD of three independent experiments (n = 3). Scale bars, 100 m.
doi:10.1371/journal.pone.0084881.g006

generated from hiPSCs when all of the factors required for differentiation are provided by chemical compounds.

Conclusion

The small molecule method can be used to rapidly, efficiently and consistently produce IM cells from multiple hiPSC/ESC lines without the mesendoderm step at a relatively low cost. This differentiation method may serve as a powerful tool for elucidating the mechanisms of mesoderm and kidney development as well as supplying cell sources for the development of regenerative medicine strategies for treating CKD.

Supporting Information

Figure S1 Mesendoderm Cells Can be Induced by the Treatment with CHIR99021 Alone. (A) Induction of BRACHYURY$^+$ cells from OSR1-GFP knock-in hiPSCs (3D45) on culture days 2, 3, 4, and 5, with or without CHIR99021. (B) mRNA expression of the mesendoderm marker genes, *BRACHYURY*, *GOOSECOID*, and *MIXL1*, in 3D45 cells treated for three days, with or without CHIR99021. 3D45 cells on day 1, before treatment, were used to normalize the data. The data shown are means ± SD of three independent experiments (n = 3). Scale bars, 100 μm.
(TIF)

Figure S2 The Small Molecule Methods Can Rapidly and Efficiently Produce IM Cells from hiPSCs. (A) Induction of OSR1$^+$ cells generated by the AM580, TTNPB, and growth factor methods. (B) Numbers of OSR1$^+$ and total cells induced by the AM580 method. The data shown are means ± SD of three independent experiments (n = 3).
(TIF)

Figure S3 The Small Molecule Methods Can be Applied to Multiple hiPSC/ESC Lines. Expression levels of *OSR1* were analyzed by qRT-PCR and compared for five hiPSC lines (3D45 [201B7], 201B6, 253G1, 253G4, and 585A1), and three hESC lines (khES1, khES3, and H9), treated for five days by the AM580 or TTNPB method, and an hiPSC line (3D45), treated for 10 days by the growth factor method. The samples of

undifferentiated hiPSCs or hESCs on day 1 before the treatment of each hiPSC or hESC line were used to normalize the data. The data shown are means ± SD of three independent experiments (n = 3).
(EPS)

Figure S4 Effects of 18 Inhibitors on Differentiation of OSR1$^+$ IM Cells by the Small Molecule Method. Effects of adding 18 signaling pathway inhibitors on induction of OSR1$^+$ cells generated by the TTNPB method. The inhibitors were added to Stage 2. The data are means ± SD on culture day 6 of three independent experiments (n = 3).
(EPS)

Figure S5 Schematic of the Differentiation Methods for inducing IM Cells from hiPSCs/ESCs. The two differentiation protocols used to induce IM cells from hiPSCs/ESCs are shown: small molecule and growth factor methods. Note that the small molecule methods induce IM cells more rapidly than the growth factor method.
(EPS)

Table S1 Binding Constants and Transactivation Properties of the Retinoids Used in the Present Study. Kd values of the six retinoids are shown for the RARα, RARβ, RARγ, and RXRα receptor isotypes.
(PDF)

Table S2 Primer Sequences Used in This Study.
(PDF)

Table S3 Antibodies and Lectins Used in This Study.
(PDF)

Table S4 Growth Factors and Chemical Compounds Used in This Study.
(PDF)

Acknowledgments

We are grateful to Dr. Takafumi Toyohara, Dr. Tatsuyuki Inoue, Dr. Fumihiko Shiota, Dr. Tetsuhiko Yasuno, Dr. Maki Kotaka, Dr. Michinori Funato, Dr. Taro Toyoda, Dr. Takahiro Sato, Dr. Akitsu Hotta, Dr. Knut Woltjen, Dr. So Nakamura and Dr. Koji Eto for technical supports and helpful suggestions; Dr. Yasunori Sato for statistical analysis; Dr. Asuka Morizane for providing the cDNA samples of neural progenitor cells induced by SFEBq culture; Tomomi Sudo, Sayaka Arai and Nanaka Gotoda-Nishimura for technical assistance.

Author Contributions

Conceived and designed the experiments: TA SM MU AO SY KO. Performed the experiments: TA SM YK. Analyzed the data: TA SM SY KO. Contributed reagents/materials/analysis tools: SY KO. Wrote the paper: TA KO.

References

1. Coresh J, Selvin E, Stevens LA, Manzi J, Kusek JW, et al. (2007) Prevalence of chronic kidney disease in the United States. JAMA 298: 2038–2047.
2. Lysaght MJ (2002) Maintenance dialysis population dynamics: current trends and long-term implications. J Am Soc Nephrol 13 Suppl 1: S37–40.
3. Matsushita K, van der Velde M, Astor BC, Woodward M, Levey AS, et al. (2010) Association of estimated glomerular filtration rate and albuminuria with all-cause and cardiovascular mortality in general population cohorts: a collaborative meta-analysis. Lancet 375: 2073–2081.
4. Evans MJ, Kaufman MH (1981) Establishment in culture of pluripotential cells from mouse embryos. Nature 292: 154–156.
5. Martin GR (1981) Isolation of a pluripotent cell line from early mouse embryos cultured in medium conditioned by teratocarcinoma stem cells. Proc Natl Acad Sci U S A 78: 7634–7638.
6. Thomson JA, Itskovitz-Eldor J, Shapiro SS, Waknitz MA, Swiergiel JJ, et al. (1998) Embryonic stem cell lines derived from human blastocysts. Science 282: 1145–1147.
7. Takahashi K, Tanabe K, Ohnuki M, Narita M, Ichisaka T, et al. (2007) Induction of pluripotent stem cells from adult human fibroblasts by defined factors. Cell 131: 861–872.
8. Takahashi K, Yamanaka S (2006) Induction of pluripotent stem cells from mouse embryonic and adult fibroblast cultures by defined factors. Cell 126: 663–676.
9. Yu J, Vodyanik MA, Smuga-Otto K, Antosiewicz-Bourget J, Frane JL, et al. (2007) Induced pluripotent stem cell lines derived from human somatic cells. Science 318: 1917–1920.
10. Kobayashi A, Valerius MT, Mugford JW, Carroll TJ, Self M, et al. (2008) Six2 defines and regulates a multipotent self-renewing nephron progenitor population throughout mammalian kidney development. Cell Stem Cell 3: 169–181.
11. Osafune K, Takasato M, Kispert A, Asashima M, Nishinakamura R (2006) Identification of multipotent progenitors in the embryonic mouse kidney by a novel colony-forming assay. Development 133: 151–161.
12. Dressler GR (2009) Advances in early kidney specification, development and patterning. Development 136: 3863–3874.
13. Saxen L (1987) Organogenesis of the Kidney. Cambridge: Cambridge University Press.
14. Mugford JW, Sipila P, McMahon JA, McMahon AP (2008) Osr1 expression demarcates a multi-potent population of intermediate mesoderm that undergoes progressive restriction to an Osr1-dependent nephron progenitor compartment within the mammalian kidney. Dev Biol 324: 88–98.
15. James RG, Kamei CN, Wang Q, Jiang R, Schultheiss TM (2006) Odd-skipped related 1 is required for development of the metanephric kidney and regulates formation and differentiation of kidney precursor cells. Development 133: 2995–3004.
16. Wang Q, Lan Y, Cho ES, Maltby KM, Jiang R (2005) Odd-skipped related 1 (Odd 1) is an essential regulator of heart and urogenital development. Dev Biol 288: 582–594.
17. D'Amour KA, Bang AG, Eliazer S, Kelly OG, Agulnick AD, et al. (2006) Production of pancreatic hormone-expressing endocrine cells from human embryonic stem cells. Nat Biotechnol 24: 1392–1401.
18. Gadue P, Huber TL, Paddison PJ, Keller GM (2006) Wnt and TGF-beta signaling are required for the induction of an in vitro model of primitive streak formation using embryonic stem cells. Proc Natl Acad Sci U S A 103: 16806–16811.
19. Mae S, Shono A, Shiota F, Yasuno T, Kajiwara M, et al. (2013) Monitoring and robust induction of nephrogenic intermediate mesoderm from human pluripotent stem cells. Nat Commun 4: 1367.
20. Borowiak M, Maehr R, Chen S, Chen AE, Tang W, et al. (2009) Small molecules efficiently direct endodermal differentiation of mouse and human embryonic stem cells. Cell Stem Cell 4: 348–358.
21. Chen S, Borowiak M, Fox JL, Maehr R, Osafune K, et al. (2009) A small molecule that directs differentiation of human ESCs into the pancreatic lineage. Nat Chem Biol 5: 258–265.
22. Wu X, Ding S, Ding Q, Gray NS, Schultz PG (2004) Small molecules that induce cardiomyogenesis in embryonic stem cells. J Am Chem Soc 126: 1590–1591.
23. Brennan HC, Nijjar S, Jones EA (1999) The specification and growth factor inducibility of the pronephric glomus in Xenopus laevis. Development 126: 5847–5856.
24. Moriya N, Uchiyama H, Asashima M (1993) Induction of pronephric tubules by activin and retinoic acid in presumptive ectoderm of xenopus laevis Dev Growth Differ 35: 123–128.
25. Osafune K, Nishinakamura R, Komazaki S, Asashima M (2002) In vitro induction of the pronephric duct in Xenopus explants. Dev Growth Differ 44: 161–167.
26. Nishikawa M, Yanagawa N, Kojima N, Yuri S, Hauser PV, et al. (2012) Stepwise renal lineage differentiation of mouse embryonic stem cells tracing in vivo development. Biochem Biophys Res Commun 417: 897–902.
27. Kim D, Dressler GR (2005) Nephrogenic factors promote differentiation of mouse embryonic stem cells into renal epithelia. J Am Soc Nephrol 16: 3527–3534.
28. Ren X, Zhang J, Gong X, Niu X, Zhang X, et al. (2010) Differentiation of murine embryonic stem cells toward renal lineages by conditioned medium from ureteric bud cells in vitro. Acta Biochim Biophys Sin (Shanghai) 42: 464–471.
29. Oeda S, Hayashi Y, Chan T, Takasato M, Aihara Y, et al. (2013) Induction of intermediate mesoderm by retinoic acid receptor signaling from differentiating mouse embryonic stem cells. Int J Dev Biol 57: 383–389.
30. Batchelder CA, Lee CC, Matsell DG, Yoder MC, Tarantal AF (2009) Renal ontogeny in the rhesus monkey (Macaca mulatta) and directed differentiation of human embryonic stem cells towards kidney precursors. Differentiation 78: 45–56.
31. Song B, Smink AM, Jones CV, Callaghan JM, Firth SD, et al. (2012) The directed differentiation of human iPS cells into kidney podocytes. PLoS One 7: e46453.

32. James RG, Schultheiss TM (2005) Bmp signaling promotes intermediate mesoderm gene expression in a dose-dependent, cell-autonomous and translation-dependent manner. Dev Biol 288: 113–125.
33. Obara-Ishihara T, Kuhlman J, Niswander L, Herzlinger D (1999) The surface ectoderm is essential for nephric duct formation in intermediate mesoderm. Development 126: 1103–1108.
34. Kajiwara M, Aoi T, Okita K, Takahashi R, Inoue H, et al. (2012) Donor-dependent variations in hepatic differentiation from human-induced pluripotent stem cells. Proc Natl Acad Sci U S A 109: 12538–12543.
35. Nakagawa M, Koyanagi M, Tanabe K, Takahashi K, Ichisaka T, et al. (2008) Generation of induced pluripotent stem cells without Myc from mouse and human fibroblasts. Nat Biotechnol 26: 101–106.
36. Suemori H, Yasuchika K, Hasegawa K, Fujioka T, Tsuneyoshi N, et al. (2006) Efficient establishment of human embryonic stem cell lines and long-term maintenance with stable karyotype by enzymatic bulk passage. Biochem Biophys Res Commun 345: 926–932.
37. McMahon AP, Bradley A (1990) The Wnt-1 (int-1) proto-oncogene is required for development of a large region of the mouse brain. Cell 62: 1073–1085.
38. Eiraku M, Watanabe K, Matsuo-Takasaki M, Kawada M, Yonemura S, et al. (2008) Self-organized formation of polarized cortical tissues from ESCs and its active manipulation by extrinsic signals. Cell Stem Cell 3: 519–532.
39. Unbekandt M, Davies JA (2010) Dissociation of embryonic kidneys followed by reaggregation allows the formation of renal tissues. Kidney Int 77: 407–416.
40. Davidson KC, Adams AM, Goodson JM, McDonald CE, Potter JC, et al. Wnt/beta-catenin signaling promotes differentiation, not self-renewal, of human embryonic stem cells and is repressed by Oct4. Proc Natl Acad Sci U S A 109: 4485–4490.
41. Lyu J, Jho EH, Lu W (2011) Smek promotes histone deacetylation to suppress transcription of Wnt target gene brachyury in pluripotent embryonic stem cells. Cell Res 21: 911–921.
42. Osafune K, Caron L, Borowiak M, Martinez RJ, Fitz-Gerald CS, et al. (2008) Marked differences in differentiation propensity among human embryonic stem cell lines. Nat Biotechnol 26: 313–315.
43. Watanabe K, Ueno M, Kamiya D, Nishiyama A, Matsumura M, et al. (2007) A ROCK inhibitor permits survival of dissociated human embryonic stem cells. Nat Biotechnol 25: 681–686.
44. Kastner P, Mark M, Chambon P (1995) Nonsteroid nuclear receptors: what are genetic studies telling us about their role in real life? Cell 83: 859–869.
45. Mascrez B, Mark M, Dierich A, Ghyselinck NB, Kastner P, et al. (1998) The RXRalpha ligand-dependent activation function 2 (AF-2) is important for mouse development. Development 125: 4691–4707.
46. Bernard BA, Bernardon JM, Delescluse C, Martin B, Lenoir MC, et al. (1992) Identification of synthetic retinoids with selectivity for human nuclear retinoic acid receptor gamma. Biochem Biophys Res Commun 186: 977–983.
47. Germain P, Kammerer S, Perez E, Peluso-Iltis C, Tortolani D, et al. (2004) Rational design of RAR-selective ligands revealed by RARbeta crystal stucture. EMBO Rep 5: 877–882.
48. Kim MJ, Ciletti N, Michel S, Reichert U, Rosenfield RL (2000) The role of specific retinoid receptors in sebocyte growth and differentiation in culture. J Invest Dermatol 114: 349–353.
49. Lehmann JM, Jong L, Fanjul A, Cameron JF, Lu XP, et al. (1992) Retinoids selective for retinoid X receptor response pathways. Science 258: 1944–1946.
50. Hogan BL, Thaller C, Eichele G (1992) Evidence that Hensen's node is a site of retinoic acid synthesis. Nature 359: 237–241.
51. Kinder SJ, Tsang TE, Wakamiya M, Sasaki H, Behringer RR, et al. (2001) The organizer of the mouse gastrula is composed of a dynamic population of progenitor cells for the axial mesoderm. Development 128: 3623–3634.
52. Tada S, Era T, Furusawa C, Sakurai H, Nishikawa S, et al. (2005) Characterization of mesendoderm: a diverging point of the definitive endoderm and mesoderm in embryonic stem cell differentiation culture. Development 132: 4363–4374.

Please cite this article in press as: Yoshida et al., Modeling the Early Phenotype at the Neuromuscular Junction of Spinal Muscular Atrophy Using Patient-Derived iPSCs, Stem Cell Reports (2015), http://dx.doi.org/10.1016/j.stemcr.2015.02.010

Stem Cell Reports
Report
ISSCR
OPEN ACCESS

Modeling the Early Phenotype at the Neuromuscular Junction of Spinal Muscular Atrophy Using Patient-Derived iPSCs

Michiko Yoshida,[1,4] Shiho Kitaoka,[2,6] Naohiro Egawa,[2,5] Mayu Yamane,[1] Ryunosuke Ikeda,[1] Kayoko Tsukita,[2] Naoki Amano,[3] Akira Watanabe,[3] Masafumi Morimoto,[4] Jun Takahashi,[1] Hajime Hosoi,[4] Tatsutoshi Nakahata,[1] Haruhisa Inoue,[2,5] and Megumu K. Saito[1,*]

[1]Department of Clinical Application
[2]Department of Cell Growth and Differentiation
[3]Department of Reprogramming Science
Center for iPS Cell Research and Application (CiRA), Kyoto University, Kyoto 606-8507, Japan
[4]Department of Pediatrics, Graduate School of Medical Science, Kyoto Prefectural University of Medicine, Kyoto 602-8566, Japan
[5]Core Research for Evolutional Science and Technology (CREST), Japan Science and Technology Agency, Saitama 332-0012, Japan
[6]Present address: Division of Pharmacology, Department of Biochemistry and Molecular Biology, Kobe University Graduate School of Medicine, Kobe 650-0017, Japan
*Correspondence: msaito@cira.kyoto-u.ac.jp
http://dx.doi.org/10.1016/j.stemcr.2015.02.010

SUMMARY

Spinal muscular atrophy (SMA) is a neuromuscular disorder caused by mutations of the *survival of motor neuron 1* (*SMN1*) gene. In the pathogenesis of SMA, pathological changes of the neuromuscular junction (NMJ) precede the motor neuronal loss. Therefore, it is critical to evaluate the NMJ formed by SMA patients' motor neurons (MNs), and to identify drugs that can restore the normal condition. We generated NMJ-like structures using MNs derived from SMA patient-specific induced pluripotent stem cells (iPSCs), and found that the clustering of the acetylcholine receptor (AChR) is significantly impaired. Valproic acid and antisense oligonucleotide treatment ameliorated the AChR clustering defects, leading to an increase in the level of full-length SMN transcripts. Thus, the current in vitro model of AChR clustering using SMA patient-derived iPSCs is useful to dissect the pathophysiological mechanisms underlying the development of SMA, and to evaluate the efficacy of new therapeutic approaches.

INTRODUCTION

Proximal spinal muscular atrophy (SMA) is an autosomal recessive neuromuscular disorder caused by the homozygous deletion or mutation of the *survival of motor neuron 1* (*SMN1*) gene, resulting in a deficiency of the ubiquitously expressed SMN protein. Patients suffer from progressive muscular weakness, which eventually results in respiratory failure in severe case. Since there are no effective treatment options, SMA remains the most frequent genetic cause of infant mortality (Burghes and Beattie, 2009; Lefebvre et al., 1995). *SMN2*, a unique gene in humans, is an almost identical copy gene of *SMN1*, but has a constitutive C to T transition in its exon 7. This transition affects the splicing of *SMN2* mRNA, thereby resulting in the predominant production of a shorter unstable isoform termed SMN-Δ7 (Monani et al., 1999). Although *SMN2* is unable to compensate for the homozygous loss of *SMN1* because of the lower amount of full-length SMN transcripts (SMN-FL), the copy number of *SMN2* affects the severity of SMA (McAndrew et al., 1997).

Based on clinical examinations and the pathological analyses of end-stage specimens, SMA historically has been described as a lower motor neuron (MN) disease characterized by the degeneration of the anterior horn cells of the spinal cord, which subsequently leads to skeletal muscle atrophy and weakness (Dubowitz, 2009). However, recent studies in SMA animal models have shown that the earliest detectable pathological change is observed at the neuromuscular junctions (NMJs), including neurofilament (NF) accumulation at the endplate on postnatal day 1 (Ling et al., 2012). Subsequently, a central synaptic defect is observed on day 4, motor neuronal loss manifests around day 9, and almost all mice die by day 15 (Sleigh et al., 2011). Therefore, impairment of the NMJ structure appears to be one of the most important phenotypes, and the development of agents that target the NMJ pathology may represent an attractive approach for therapy. Indeed, an aberrant ultrastructure of NMJs also has been reported in a human prenatal specimen obtained from a fetus with type I SMA (Martínez-Hernández et al., 2013).

Despite recent advances in our understanding of the disease, the detailed mechanism(s) involved in the NMJ formation and maturation, which occur during both the prenatal and early postnatal periods, have not been fully described (Wu et al., 2012). With a few exceptions, the analyses of the pathological roles of SMN have been conducted mainly using animal models, because there are difficulties associated with obtaining human specimens from either biopsy or post-mortem samples. Although there are several available transgenic mouse models of SMA, inter-species differences between mice and humans, such as the

Please cite this article in press as: Yoshida et al., Modeling the Early Phenotype at the Neuromuscular Junction of Spinal Muscular Atrophy Using Patient-Derived iPSCs, Stem Cell Reports (2015), http://dx.doi.org/10.1016/j.stemcr.2015.02.010

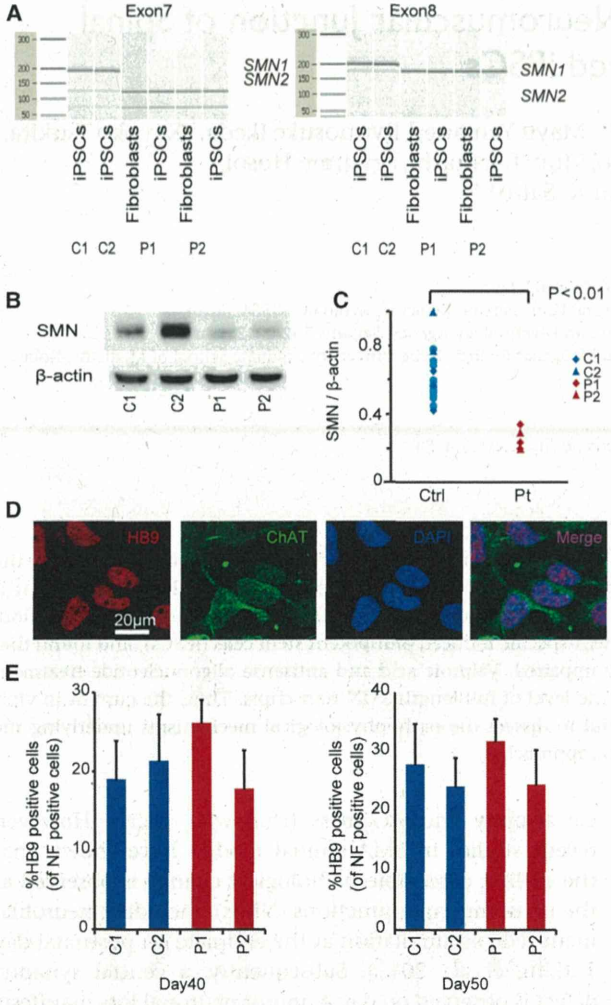

Figure 1. Differentiation of iPSCs into Spinal MNs

(A) The PCR restriction fragment-length polymorphism (RFLP) analysis using a bioanalyzer confirmed that the SMA-iPSCs maintained exon 7 and 8 deletions in the *SMN1* gene.

(B) Western blot analysis of SMN proteins.

(C) Quantification of the SMN protein expression relative to that of β-actin (eight control PSC clones and two SMA-iPSC clones) (n = 3, Wilcoxon rank-sum test).

(D) Immunostaining of SMA-iPSC-derived MNs. HB9, red; and ChAT, green on day 60.

(E) The quantitative immunocytochemical analysis for HB9-positive iPSC-derived MNs (means ± SEM, n = 3). See also Figure S1.

existence of *SMN2* in humans, hamper the translation of the findings in mouse studies to human clinical trials (Harahap et al., 2012; Martínez-Hernández et al., 2009; Park et al., 2010). Furthermore, there are difficulties related to evaluating the pathological roles of neurons and myocytes separately. To establish a platform to elucidate the pathology of the NMJ in SMA patients, we herein evaluated the ability of MNs from SMA patient-derived induced pluripotent stem cells (iPSCs) (Takahashi et al., 2007) to form NMJs.

RESULTS

Generation and Characterization of iPSCs from Type 1 SMA Patients

Fibroblasts from two independent type 1 SMA patients (Coriell IDs GM00232 and GM03813, referred to as P1 and P2) were reprogrammed by episomal vectors (Okita et al., 2011). Both SMA-iPSC clones used in this study (P1 and P2) showed a characteristic human embryonic stem cell (ESC)-like morphology, and expressed pluripotent markers compared to control ESC (KhES1) and iPSCs (201B7 and 409B2, referred to as C1 and C2) (Figures S1A and S1B). The RNA microarray analysis confirmed that the global gene expression pattern (Figures S1C and S1D) and levels of pluripotent stem cell-related genes (Figure S1E) in the P1 and P2 iPSCs were similar to that observed in the control iPSCs. The P1 and P2 iPSCs also exhibited demethylation of NANOG and OCT3/4 loci (Figure S1F) and maintained a normal karyotype (Figure S1G). Pluripotency of P1 and P2 iPSC lines were confirmed by teratoma formation assay (Figure S1H). The expression of introduced transgenes was rarely detected (Figure S1I). The genetic identity of the iPSC clones was proven by a short tandem repeat analysis (data not shown). SMA-iPSCs were confirmed to carry homozygosis deletions of exons 7 and 8 of the *SMN1* gene (Figure 1A; van der Steege et al., 1995), and their SMN protein level was also significantly lower than that in control iPSCs, including C1 and C2 (Figures 1B and 1C).

MN Differentiation of SMA-iPSCs

We next directed the SMA- and control iPSCs to differentiate into MNs using a previously reported cortical neuron (Morizane et al., 2011) and spinal MN differentiation protocol, with some modifications (Egawa et al., 2012). The iPSC-derived neurons expressed neuronal markers (Figure S2A) and MN-specific markers (Figure 1D). The expression of the introduced transgene *OCT3/4* detected in the P1-iPSCs was completely silenced after 40 days of MN differentiation (Figure S2B). Although a significant decline in MNs over time has been reported as a hallmark of SMA patient iPSC-derived MNs (Chang et al., 2011; Corti et al., 2012; Ebert et al., 2009), the two independent SMA-iPSC lines produced and maintained a similar number of HB9-positive MNs compared to control iPSCs after 40 and 50 days of differentiation (Figure 1E). Therefore, in our MN differentiation system, the SMA-iPSC lines were competent in generating mature MNs and presented no evidence of cell-autonomous MN loss by 50 days of differentiation.

Please cite this article in press as: Yoshida et al., Modeling the Early Phenotype at the Neuromuscular Junction of Spinal Muscular Atrophy Using Patient-Derived iPSCs, Stem Cell Reports (2015), http://dx.doi.org/10.1016/j.stemcr.2015.02.010

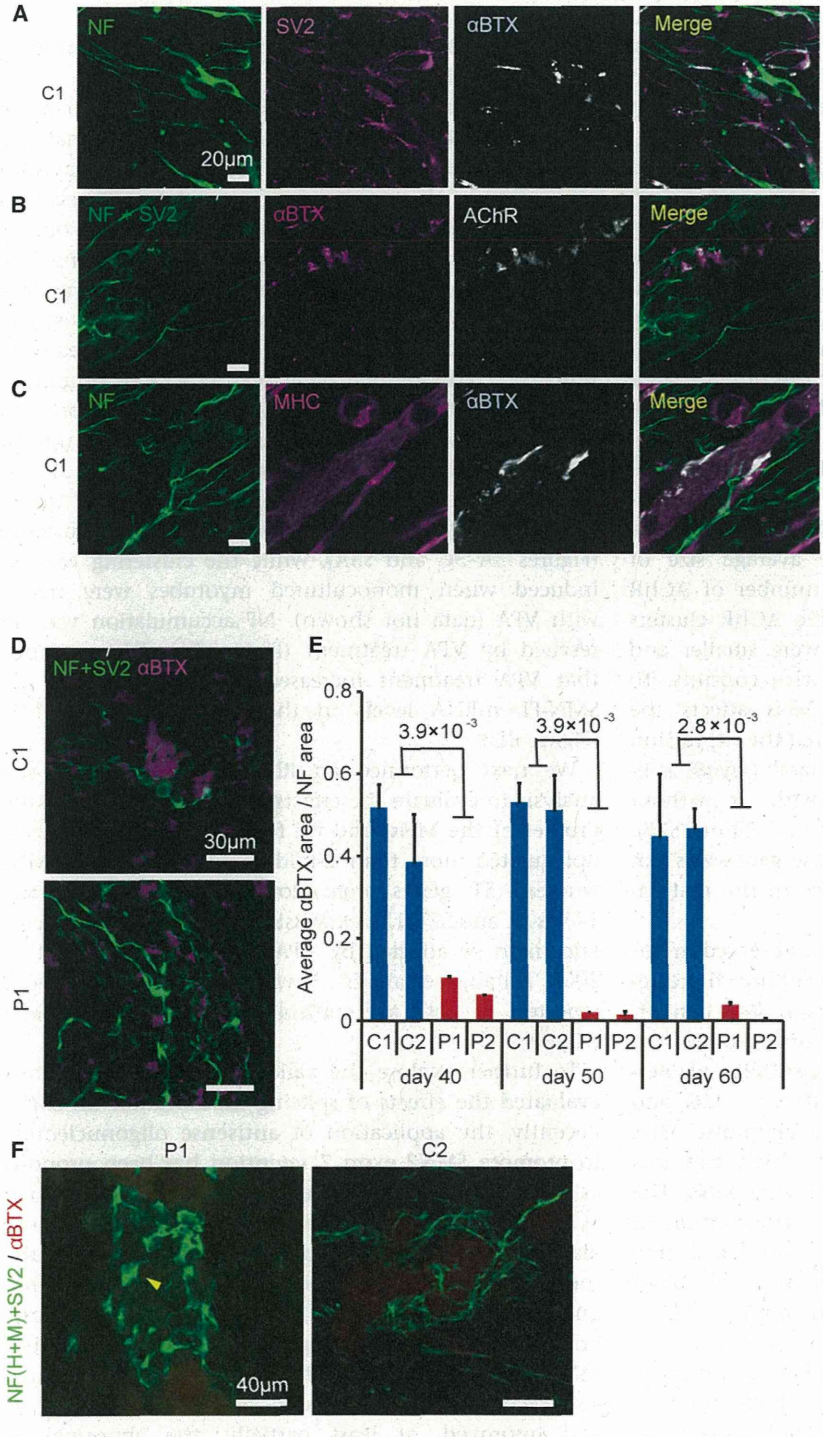

Figure 2. The Pre- and Post-synaptic Morphological Defects in Type 1 SMA

(A–D) Representative confocal micrographs showing the immunocytochemically labeled NMJ-LSs of iPSC-derived neurons and C2C12 myotubes. (A and B) Representative images of AChR clusters formed by C1 MNs. (C) AChR clusters stained with MHC. (D) NMJ-LSs of patient (P1)- and control (C1)-derived MNs on day 60.

(E) Quantitative immunocytochemical analysis of the α-BTX-positive area (means ± SEM, n = 3, Wilcoxon rank-sum test).

(F) Abnormal NF accumulation (yellow arrows) and poor terminal arborization of MNs in the SMA NMJ-LSs. See also Figure S2.

Formation of NMJ-like Structure with SMA-iPSCs

We next tried to develop an in vitro NMJ formation model using the human iPSC-derived MNs. We co-cultured control MNs with differentiated murine C2C12 cell lines and found that αBTX-positive AChRs were clustered at the site of SV2-positive neuronal endplates (Figure 2A). To exclude the presence of unexpected artifacts of αBTX staining under these conditions, we co-stained samples

Please cite this article in press as: Yoshida et al., Modeling the Early Phenotype at the Neuromuscular Junction of Spinal Muscular Atrophy Using Patient-Derived iPSCs, Stem Cell Reports (2015), http://dx.doi.org/10.1016/j.stemcr.2015.02.010

with αBTX and anti-AChR antibodies and confirmed that the regions of both positive staining merged completely (Figure 2B). In addition, the AChR clusters were localized on myosin heavy chain (MHC)-positive multinuclear myotubes (Figure 2C).

We next evaluated the AChR clustering on myotubes co-cultured with SMA-iPSC-derived MNs and found it remarkably impaired (Figure 2D). We evaluated the area of αBTX to assess the ability of MNs to form and maintain the NMJ-like structures (NMJ-LSs). We evaluated the AChR clustering at several time points to determine whether MN maturation affects the phenotype of the NMJ-LSs. The SMA-iPSC-derived MNs induced far less AChR clustering in myotubes than control iPSC-derived MNs did at 40, 50, or 60 days of differentiation (Figures 2E and S2C). AChR clustering was rarely observed for either the SMA- or control iPSC-derived MNs at time points earlier than day 30 (data not shown). We also evaluated the average size of each AChR cluster (Figure S2D) and number of AChR clusters (Figure S2E). Consequently, the AChR clusters formed with SMA-iPSC-derived MNs were smaller and fewer in number than those formed with controls. To evaluate whether co-culturing with MNs affects the maturation status of C2C12, we compared the expression levels of embryonic (*Myh3*) and perinatal (*Myh8*) subtypes of MHCs in skeletal muscle with or without co-culturing (Stern-Straeter et al., 2011; Figure S2F). However, the ratio of expression of these genes was not different, indicating a lack of difference in the maturation of C2C12.

Although motor neuronal loss was not observed in our MN differentiation system without co-culture, there remains a possibility that the NMJ defects in SMA patient-derived MNs are due to MN death occurring under the co-culture conditions. To exclude the possibility, we performed TUNEL staining of the MNs (Figures S2G and S2H). The number of TUNEL-positive apoptotic MNs did not increase during co-culturing, which confirms that synapse loss indeed occurs in surviving MNs. The accumulation of NF proteins and poor arborization in distal axons and motor nerve terminals are considered to be specific features of SMA model mice, although their significance in the pathogenesis of human SMA is unknown (Cifuentes-Diaz et al., 2002; Kariya et al., 2008; Kong et al., 2009). These findings were observed in SMA-iPSC-derived MNs (Figure 2F), which indicates the functional deficit of the motor endplate in SMA. Taken together, the SMA-iPSC-derived MNs had impaired AChR clustering on myotubes in the absence of MN loss, indicating that there was functional impairment of MNs in terms of their forming or allowing for the maturation of NMJs.

The SMA Phenotype in NMJ-LS Was Rescued by Valproic Acid and Phosphorodiamidate Morpholino Oligonucleotides

Since the loss of NMJ formation is regarded to be an important hallmark preceding the motor neuronal loss, compounds that ameliorate the NMJ pathology may serve as promising therapeutic drug candidates. To evaluate whether the NMJ-LSs formation system used in our experiments can serve as a prototype for evaluating drug candidates, we assessed whether the SMN-inducing drug, valproic acid (VPA), could increase the AChR clustering in our co-culture system. VPA is known to increase the functional SMN protein by activating various promoters, including that of *SMN2*, and by correcting the abnormal splicing of *SMN2* exon 7, mainly through the upregulation of splicing factors (Harahap et al., 2012). Co-culturing myotubes and SMA-iPSC-derived MNs treated with VPA significantly increased the AChR clustering (Figures 3A–3C and S3A), while the clustering was not induced when monocultured myotubes were treated with VPA (data not shown). NF accumulation was not rescued by VPA treatment (Figure 3A). We confirmed that VPA treatment increased both the SMN-Δ7 and SMN-FL mRNA levels in the SMA-iPSC-derived MNs (Figure 3D).

We next performed an RNA sequencing (RNA-seq) analysis to evaluate the effects of VPA on the expression profiles of the MNs, and we found 227 genes that were upregulated more than 2-fold in the VPA-treated MNs, whereas 51 genes were downregulated (Figure S3B; Tables S1 and S2). The expression levels of splicing factors known to be affected by VPA treatment (Brichta et al., 2003; Harahap et al., 2012) were slightly upregulated as reported, in both the control and patient-derived MNs (Figure S3C).

To further explore the validity of NMJ-LSs, we next evaluated the effects of splicing modification on *SMN2*. Recently, the application of antisense oligonucleotides to promote *SMN2* exon 7 retention has been proposed as an alternative therapeutic approach for SMA (Mitrpant et al., 2013). For this purpose, we introduced phosphorodiamidate morpholino oligonucleotides (PMOs) targeting the intronic silencing motif in *SMN2* intron 7. Consequently, the SMN-specific PMO treatment dramatically improved AChR clustering with the patient-derived MNs (Figures 4A, 4B, and S3D). The PMO treatment also recovered the expression of SMN-FL (Figure 4C) and improved, at least partially, the abnormal NF accumulation (Figure 4A). We consider that these data indicate the potential therapeutic advantages of PMO for SMA patients. Overall, the NMJ-LS morphology could be useful for evaluating new therapeutic approaches for SMA.

Please cite this article in press as: Yoshida et al., Modeling the Early Phenotype at the Neuromuscular Junction of Spinal Muscular Atrophy Using Patient-Derived iPSCs, Stem Cell Reports (2015), http://dx.doi.org/10.1016/j.stemcr.2015.02.010

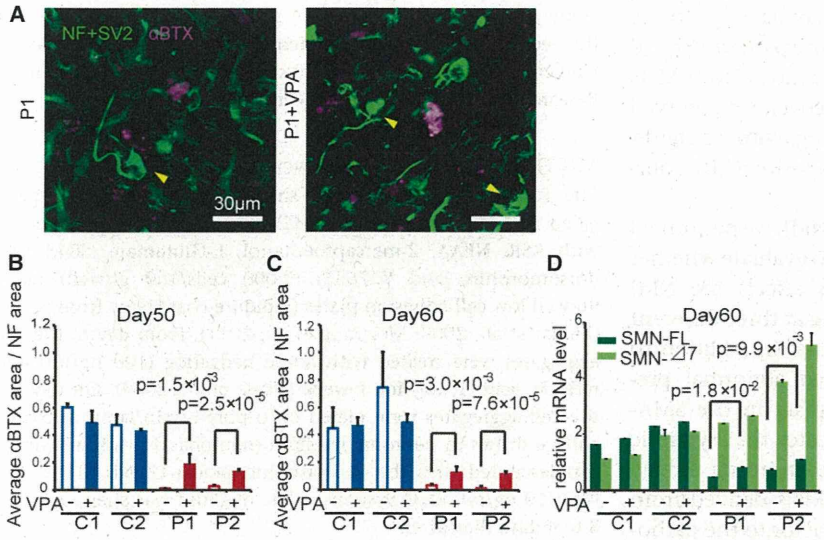

Figure 3. VPA Treatment Rescues the NMJ Pathology in SMA Patient-Derived Cell Cultures

(A) Representative images of NMJ-LSs formed with or without VPA. Yellow arrows indicate abnormal NF accumulation.

(B and C) Quantitative immunocytochemical analysis of the α-BTX area after VPA treatment (1 mM) (means ± SEM, n = 3, Student's t test).

(D) The mRNA levels of SMN-FL and SMN-Δ7 in SMA-iPSC MNs (means ± SEM, n = 3, Student's t test). See also Figure S3 and Tables S1 and S2.

DISCUSSION

Previous studies regarding the phenotype of MNs differentiated from SMA-iPSCs have focused mainly on the cell autonomous defects, such as shortened neurite extension, and the reduced size of the cell body; but, their significance in relation to the in vivo phenotype remains unclear (Chang et al., 2011; Ebert et al., 2009). Although motor neuronal loss during culture also has been reported, this is not observed in vivo until the end stage of the disease. We did not observe any progressive motor neuronal loss during culture, even during the longer time period, which is contrary to the previous reports (Chang et al., 2011; Corti et al., 2012; Ebert et al., 2009; Sareen et al., 2012). The precise reason for this difference is unknown, but a variety of methodological differences during culture, such as difference in the timing of the analysis, the protocol of MN differentiation, and the methods used for the evaluation, could all have contributed to this phenotypic variation. Although Corti et al. briefly reported the detection of NMJ defects after co-culturing human myoblasts and SMA-iPSC-derived MNs in a recent report (Corti et al., 2012), MN loss was observed without co-culturing the cells with myotubes in their SMA model, leaving the possibility

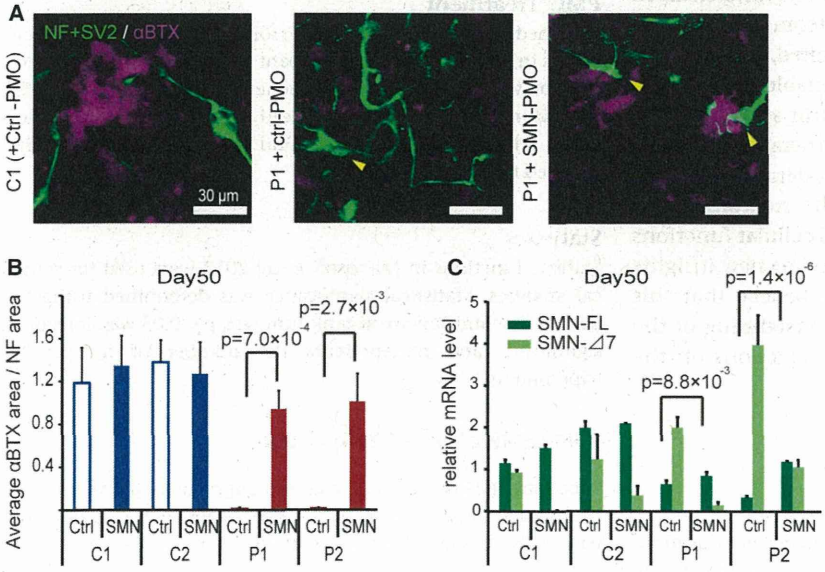

Figure 4. PMO Treatment Rescues the NMJ Pathology in SMA Patient-Derived Cell Cultures

(A) Representative images of NMJ-LSs formed with or without PMOs. Yellow arrows indicate abnormal NF accumulation.

(B) Quantitative immunocytochemical analysis of the α-BTX area after PMO treatment (means ± SEM, n = 3, Student's t test).

(C) The mRNA levels of SMN-FL and SMN-Δ7 with PMO treatment (means ± SEM, n = 3, Student's t test). See also Figure S3.

Please cite this article in press as: Yoshida et al., Modeling the Early Phenotype at the Neuromuscular Junction of Spinal Muscular Atrophy Using Patient-Derived iPSCs, Stem Cell Reports (2015), http://dx.doi.org/10.1016/j.stemcr.2015.02.010

that preceding motor neuronal death may have led to the defect in forming the NMJ. In contrast, the patient-derived iPSCs used in our study yielded a similar ratio of HB9+ MNs compared to the two control lines. Moreover, we observed a significant reduction in AChR clustering, with no significant increases in the number of TUNEL-positive MNs, during co-culturing.

Since we focused on the pathology of NMJ, we performed a detailed examination of our NMJ-LS. To evaluate whether the developmental status of the MNs affects the NMJ pathology, we evaluated AChR clustering at three different time points and obtained consistent data. In addition to impaired AChR clustering, we detected abnormal presynaptic NF accumulation at the endplate in the SMA-iPSC-derived neurons, which also indicates that synaptic breakdown precedes motor neuronal death in our model. These data support a hypothesis that MNs derived from patient iPSCs are a major contributing factor to the pathogenesis in the NMJ due to SMA. Based on these observations, we considered that the morphological defect of NMJ-LS in our culture was due to functional impairments of the MNs in target pathfinding and/or in inducing or maintaining AChR clustering, rather than due to motor neuronal loss. Considering that the formation and maintenance of NMJs has been indicated to precede the occurrence of MN death even in humans, as mentioned above, the vulnerability of MNs in SMA patients seems to be due not only to the autonomous cell susceptibility to various stresses, but also as a consequence of the NMJ defect, which causes the impairment of neurotrophic factors and subsequent death of MNs (Fidziańska and Rafalowska, 2002; Fischer et al., 2004).

In summary, we demonstrated that the early SMA phenotype in NMJ could be recapitulated with MN differentiated from SMA-iPSCs. Since the available outcome measures to assess the drug efficacy in SMA are limited, our findings that the NMJ is a vulnerable target amenable to rescue by VPA and PMOs seems to indicate that this system will be useful for future evaluations of novel therapeutic candidates. Further experiments with patient-derived iPSCs on the neurodevelopmental aspects of the neuromuscular system, including specific molecular and cellular functions of SMN in both muscle and MN, will provide new insights into the pathophysiology of SMA. We believe that this approach will also help deepen our understanding of the pathogenesis of the muscle and MN interactions on the formation of the NMJ.

EXPERIMENTAL PROCEDURES

Study Approval

Use of human ESCs was approved by the Ministry of Education, Culture, Sports, Science and Technology of Japan (MEXT). The study plan for recombinant DNA research has been approved by the recombinant DNA experiments safety committee of Kyoto University. An experimental protocol was approved by the Animal Research Committee of CiRA, Kyoto University.

MN Differentiation and Co-culture with C2C12

The iPSCs were dissociated into single cells and quickly re-aggregated in DFK 5% medium (DMEM/F12 medium supplemented with KSR, NEAA, 2-mercaptoethanol, L-Glutamate, SB431542, dorsomorphin, and Y27632) (9,000 cells/150 μl/well) using 96-well low cell-adhesion plates (Lipidure-coat U96w from Nunc) (Eiraku et al., 2008; Morizane et al., 2011). From day 8, the cell aggregates were treated with Sonic hedgehog (100 ng/ml) and retinoic acid (1 μM) for 1 week (Wada et al., 2009). On day 20, the cell aggregates were plated onto poly-l-lysin/laminin-coated culture dishes in neuronal medium (neurobasal medium [Gibco] supplemented with the neurotrophic factors GDNF, BDNF, and NT3 [10 ng/ml, R&D Systems]). The medium was changed every 3 to 4 days thereafter.

For the co-culture with neuronal cells, the fusion of C2C12 myoblasts was induced by switching to the differentiation medium (DMEM supplemented with horse serum). On day 4, the MNs that had differentiated from the iPSCs (differentiation days 34–54) were harvested and plated on the induced myotubes, and the medium was changed to neuronal medium. Thereafter, the cultures were fed every 2 days by changing half of the medium.

VPA Treatment

Co-cultured samples were treated with or without 1 mM VPA by changing half of the medium every 2 days. After 6 days of drug treatment, the area of NF and αBTX immunostaining was detected by immunocytochemistry and was analyzed by the IN Cell Analyzer 2000 software program.

PMO Treatment

Designed PMOs SMN2E7D(-10-29) for suppressing splice silencing motifs in intron 7 of *SMN2* (Mitrpant et al., 2013) and its negative control were purchased from Gene Tools. SMN- or Ctrl-PMO (10 μM in medium) were introduced with the Endo-Porter (Gene Tools) on day 1 of co-culturing, and the cells were subsequently cultured for 3 days.

Statistics

Statistic functions in Microsoft Excel 2013 were used for statistical analyses. Statistical significance was determined using Student's t test and Wilcoxon rank-sum test, $p < 0.05$ was considered significant, and n represents the number of independent experiments.

SUPPLEMENTAL INFORMATION

Supplemental Information includes Supplemental Experimental Procedures, three figures, and three tables and can be found with this article online at http://dx.doi.org/10.1016/j.stemcr.2015.02.010.

Please cite this article in press as: Yoshida et al., Modeling the Early Phenotype at the Neuromuscular Junction of Spinal Muscular Atrophy Using Patient-Derived iPSCs, Stem Cell Reports (2015), http://dx.doi.org/10.1016/j.stemcr.2015.02.010

AUTHOR CONTRIBUTIONS

M.Yo., S.K., M.M., H.H., J.T., T.N., H.I., and M.K.S. designed the research. M.Yo., S.K., N.E., M.Ya., R.I., N.A., and K.T. performed the research. M.Yo., A.W., M.Ya., and R.I. analyzed the data. M.Yo. and M.K.S. wrote the paper.

ACKNOWLEDGMENTS

We are grateful to Y. Sasaki, Y. Jindai, S. Nakamura, S. Benno, and T. Ohkame for their technical assistance. We also thank A. Niwa, K. Oshima, T. Tanaka, and K. Chiyonobu for scientific comments, and H. Watanabe for administrative assistance. We are grateful to Dr. Keisuke Okita for plasmid distribution and scientific comments. This work was supported by grants from Ministry of Health, Labour and Welfare of Japan; grants from the Ministry of Education, Culture, Sports, Science and Technology of Japan; the Leading Project of Ministry of Education, Culture, Sports, Science and Technology (T.N.); the Funding Program for World-Leading Innovative Research and Development on Science and Technology of the Japan Society for the Promotion of Science (T.N. and M.K.S.); the grant for Core Center for iPS Cell Research of Research Center Network for Realization of Regenerative Medicine from the Japan Science and Technology Agency (JST) (T.N., H.I, and M.K.S.); CREST (H.I.); the Ministry of Health, Labour and Welfare of Japan (H.I.); the Ministry of Education, Culture, Sports, Science and Technology of Japan (Innovative Area Foundation of Synapse and Neurocircuit Pathology [22110007] to H.I.); the Program for Intractable Diseases Research utilizing disease-specific iPS cells of JST (H.I. and T.N.); the Japan Research Foundation for Clinical Pharmacology (H.I.); the Mochida Memorial Foundation for Medical and Pharmaceutical Research (H.I.); and Intramural Research Grant (24-9) for Neurological and Psychiatry Disorders of NCNP (H.I.).

Received: October 4, 2013
Revised: February 12, 2015
Accepted: February 12, 2015
Published: March 19, 2015

REFERENCES

Brichta, L., Hofmann, Y., Hahnen, E., Siebzehnrubl, F.A., Raschke, H., Blumcke, I., Eyupoglu, I.Y., and Wirth, B. (2003). Valproic acid increases the SMN2 protein level: a well-known drug as a potential therapy for spinal muscular atrophy. Hum. Mol. Genet. *12*, 2481–2489.

Burghes, A.H., and Beattie, C.E. (2009). Spinal muscular atrophy: why do low levels of survival motor neuron protein make motor neurons sick? Nat. Rev. Neurosci. *10*, 597–609.

Chang, T., Zheng, W., Tsark, W., Bates, S., Huang, H., Lin, R.J., and Yee, J.K. (2011). Brief report: phenotypic rescue of induced pluripotent stem cell-derived motoneurons of a spinal muscular atrophy patient. Stem Cells *29*, 2090–2093.

Cifuentes-Diaz, C., Nicole, S., Velasco, M.E., Borra-Cebrian, C., Panozzo, C., Frugier, T., Millet, G., Roblot, N., Joshi, V., and Melki, J. (2002). Neurofilament accumulation at the motor endplate and lack of axonal sprouting in a spinal muscular atrophy mouse model. Hum. Mol. Genet. *11*, 1439–1447.

Corti, S., Nizzardo, M., Simone, C., Falcone, M., Nardini, M., Ronchi, D., Donadoni, C., Salani, S., Riboldi, G., Magri, F., et al. (2012). Genetic correction of human induced pluripotent stem cells from patients with spinal muscular atrophy. Sci. Transl. Med. *4*, 165ra162.

Dubowitz, V. (2009). Ramblings in the history of spinal muscular atrophy. Neuromuscul. Disord. *19*, 69–73.

Ebert, A.D., Yu, J., Rose, F.F., Jr., Mattis, V.B., Lorson, C.L., Thomson, J.A., and Svendsen, C.N. (2009). Induced pluripotent stem cells from a spinal muscular atrophy patient. Nature *457*, 277–280.

Egawa, N., Kitaoka, S., Tsukita, K., Naitoh, M., Takahashi, K., Yamamoto, T., Adachi, F., Kondo, T., Okita, K., Asaka, I., et al. (2012). Drug screening for ALS using patient-specific induced pluripotent stem cells. Sci. Transl. Med. *4*, 145ra104.

Eiraku, M., Watanabe, K., Matsuo-Takasaki, M., Kawada, M., Yonemura, S., Matsumura, M., Wataya, T., Nishiyama, A., Muguruma, K., and Sasai, Y. (2008). Self-organized formation of polarized cortical tissues from ESCs and its active manipulation by extrinsic signals. Cell Stem Cell *3*, 519–532.

Fidziańska, A., and Rafalowska, J. (2002). Motoneuron death in normal and spinal muscular atrophy-affected human fetuses. Acta Neuropathol. *104*, 363–368.

Fischer, L.R., Culver, D.G., Tennant, P., Davis, A.A., Wang, M., Castellano-Sanchez, A., Khan, J., Polak, M.A., and Glass, J.D. (2004). Amyotrophic lateral sclerosis is a distal axonopathy: evidence in mice and man. Exp. Neurol. *185*, 232–240.

Harahap, I.S., Saito, T., San, L.P., Sasaki, N., Gunadi, Nurputra, D.K., Yusoff, S., Yamamoto, T., Morikawa, S., Nishimura, N., et al. (2012). Valproic acid increases SMN2 expression and modulates SF2/ASF and hnRNPA1 expression in SMA fibroblast cell lines. Brain Dev. *34*, 213–222.

Kariya, S., Park, G.H., Maeno-Hikichi, Y., Leykekhman, O., Lutz, C., Arkovitz, M.S., Landmesser, L.T., and Monani, U.R. (2008). Reduced SMN protein impairs maturation of the neuromuscular junctions in mouse models of spinal muscular atrophy. Hum. Mol. Genet. *17*, 2552–2569.

Kong, L., Wang, X., Choe, D.W., Polley, M., Burnett, B.G., Bosch-Marcé, M., Griffin, J.W., Rich, M.M., and Sumner, C.J. (2009). Impaired synaptic vesicle release and immaturity of neuromuscular junctions in spinal muscular atrophy mice. J. Neurosci. *29*, 842–851.

Lefebvre, S., Bürglen, L., Reboullet, S., Clermont, O., Burlet, P., Viollet, L., Benichou, B., Cruaud, C., Millasseau, P., Zeviani, M., et al. (1995). Identification and characterization of a spinal muscular atrophy-determining gene. Cell *80*, 155–165.

Ling, K.K., Gibbs, R.M., Feng, Z., and Ko, C.P. (2012). Severe neuromuscular denervation of clinically relevant muscles in a mouse model of spinal muscular atrophy. Hum. Mol. Genet. *21*, 185–195.

Martínez-Hernández, R., Soler-Botija, C., Also, E., Alías, L., Caselles, L., Gich, I., Bernal, S., and Tizzano, E.F. (2009). The developmental pattern of myotubes in spinal muscular atrophy indicates prenatal delay of muscle maturation. J. Neuropathol. Exp. Neurol. *68*, 474–481.

Martínez-Hernández, R., Bernal, S., Also-Rallo, E., Alías, L., Barceló, M.J., Hereu, M., Esquerda, J.E., and Tizzano, E.F. (2013). Synaptic defects in type I spinal muscular atrophy in human development. J. Pathol. *229*, 49–61.

McAndrew, P.E., Parsons, D.W., Simard, L.R., Rochette, C., Ray, P.N., Mendell, J.R., Prior, T.W., and Burghes, A.H. (1997). Identification of proximal spinal muscular atrophy carriers and patients by analysis of SMNT and SMNC gene copy number. Am. J. Hum. Genet. *60*, 1411–1422.

Mitrpant, C., Porensky, P., Zhou, H., Price, L., Muntoni, F., Fletcher, S., Wilton, S.D., and Burghes, A.H. (2013). Improved antisense oligonucleotide design to suppress aberrant SMN2 gene transcript processing: towards a treatment for spinal muscular atrophy. PLoS ONE *8*, e62114.

Monani, U.R., Lorson, C.L., Parsons, D.W., Prior, T.W., Androphy, E.J., Burghes, A.H., and McPherson, J.D. (1999). A single nucleotide difference that alters splicing patterns distinguishes the SMA gene SMN1 from the copy gene SMN2. Hum. Mol. Genet. *8*, 1177–1183.

Morizane, A., Doi, D., Kikuchi, T., Nishimura, K., and Takahashi, J. (2011). Small-molecule inhibitors of bone morphogenic protein and activin/nodal signals promote highly efficient neural induction from human pluripotent stem cells. J. Neurosci. Res. *89*, 117–126.

Okita, K., Matsumura, Y., Sato, Y., Okada, A., Morizane, A., Okamoto, S., Hong, H., Nakagawa, M., Tanabe, K., Tezuka, K., et al. (2011). A more efficient method to generate integration-free human iPS cells. Nat. Methods *8*, 409–412.

Park, G.H., Maeno-Hikichi, Y., Awano, T., Landmesser, L.T., and Monani, U.R. (2010). Reduced survival of motor neuron (SMN) protein in motor neuronal progenitors functions cell autonomously to cause spinal muscular atrophy in model mice expressing the human centromeric (SMN2) gene. J. Neurosci. *30*, 12005–12019.

Sareen, D., Ebert, A.D., Heins, B.M., McGivern, J.V., Ornelas, L., and Svendsen, C.N. (2012). Inhibition of apoptosis blocks human motor neuron cell death in a stem cell model of spinal muscular atrophy. PLoS ONE *7*, e39113.

Sleigh, J.N., Gillingwater, T.H., and Talbot, K. (2011). The contribution of mouse models to understanding the pathogenesis of spinal muscular atrophy. Dis. Model. Mech. *4*, 457–467.

Stern-Straeter, J., Bonaterra, G.A., Kassner, S.S., Zügel, S., Hörmann, K., Kinscherf, R., and Goessler, U.R. (2011). Characterization of human myoblast differentiation for tissue-engineering purposes by quantitative gene expression analysis. J. Tissue Eng. Regen. Med. *5*, e197–e206.

Takahashi, K., Tanabe, K., Ohnuki, M., Narita, M., Ichisaka, T., Tomoda, K., and Yamanaka, S. (2007). Induction of pluripotent stem cells from adult human fibroblasts by defined factors. Cell *131*, 861–872.

van der Steege, G., Grootscholten, P.M., van der Vlies, P., Draaijers, T.G., Osinga, J., Cobben, J.M., Scheffer, H., and Buys, C.H. (1995). PCR-based DNA test to confirm clinical diagnosis of autosomal recessive spinal muscular atrophy. Lancet *345*, 985–986.

Wada, T., Honda, M., Minami, I., Tooi, N., Amagai, Y., Nakatsuji, N., and Aiba, K. (2009). Highly efficient differentiation and enrichment of spinal motor neurons derived from human and monkey embryonic stem cells. PLoS ONE *4*, e6722.

Wu, H., Lu, Y., Shen, C., Patel, N., Gan, L., Xiong, W.C., and Mei, L. (2012). Distinct roles of muscle and motoneuron LRP4 in neuromuscular junction formation. Neuron *75*, 94–107.

Stem Cell Reports, Volume *4*
Supplemental Information

Modeling the Early Phenotype at the Neuromuscular Junction of Spinal Muscular Atrophy Using Patient-Derived iPSCs

Michiko Yoshida, Shiho Kitaoka, Naohiro Egawa, Mayu Yamane, Ryunosuke Ikeda, Kayoko Tsukita, Naoki Amano, Akira Watanabe, Masafumi Morimoto, Jun Takahashi, Hajime Hosoi, Tatsutoshi Nakahata, Haruhisa Inoue, and Megumu K. Saito

Figure S1

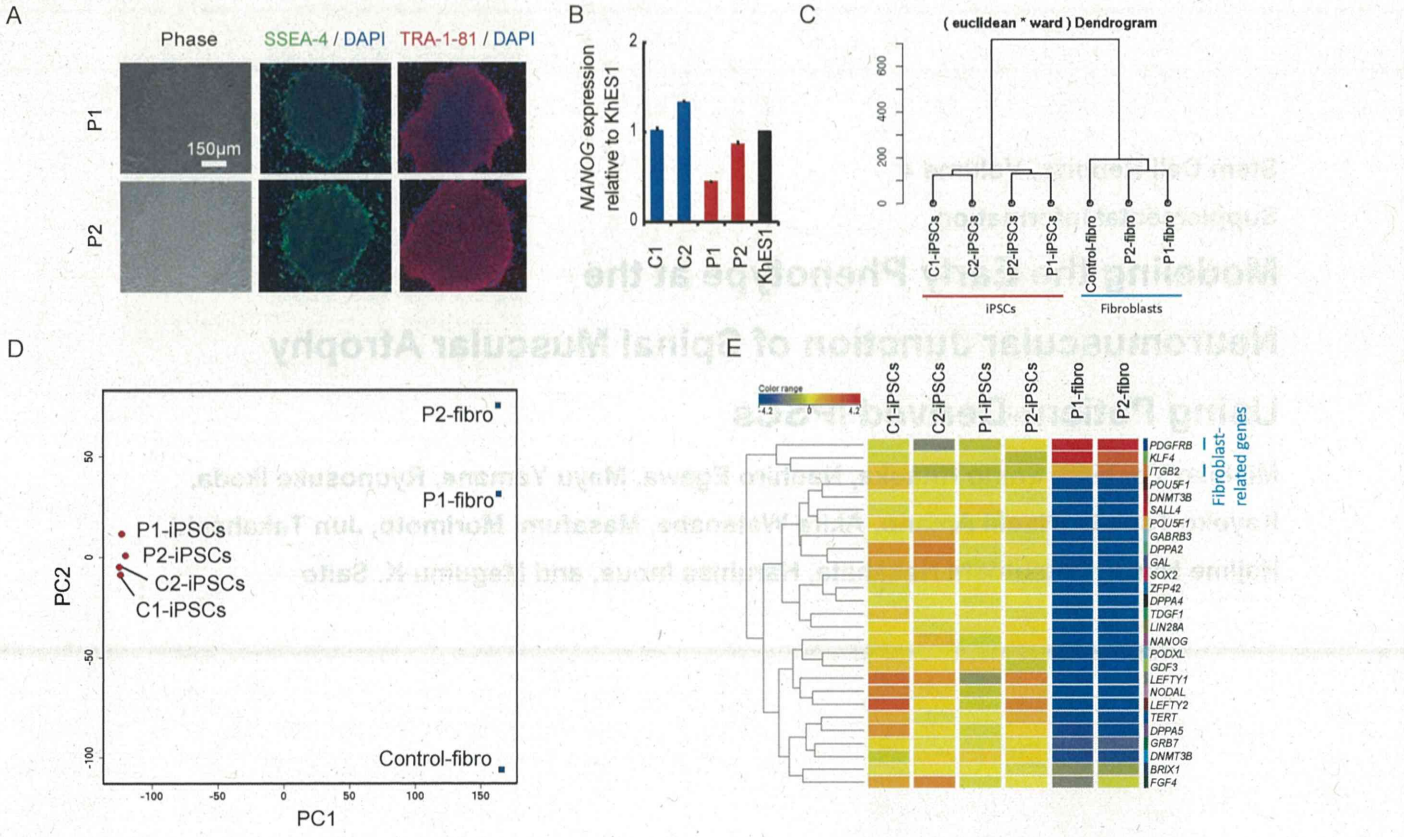
A
Phase
SSEA-4 / DAPI
TRA-1-81 / DAPI
P1
P2
150µm
B
NANOG expression relative to KhES1
C1
C2
P1
P2
KhES1
C
(euclidean * ward) Dendrogram
C1-iPSCs
C2-iPSCs
P2-iPSCs
P1-iPSCs
Control-fibro
P2-fibro
P1-fibro
iPSCs
Fibroblasts
D
P2-fibro
P1-fibro
P1-iPSCs
P2-iPSCs
C2-iPSCs
C1-iPSCs
Control-fibro
PC2
PC1
E
Color range
C1-iPSCs
C2-iPSCs
P1-iPSCs
P2-iPSCs
P1-fibro
P2-fibro
PDGFRB
KLF4
ITGB2
POU5F1
DNMT3B
SALL4
POU5F1
GABRB3
DPPA2
GAL
SOX2
ZFP42
DPPA4
TDGF1
LIN28A
NANOG
PODXL
GDF3
LEFTY1
NODAL
LEFTY2
TERT
DPPA5
GRB7
DNMT3B
BRIX1
FGF4
Fibroblast-related genes

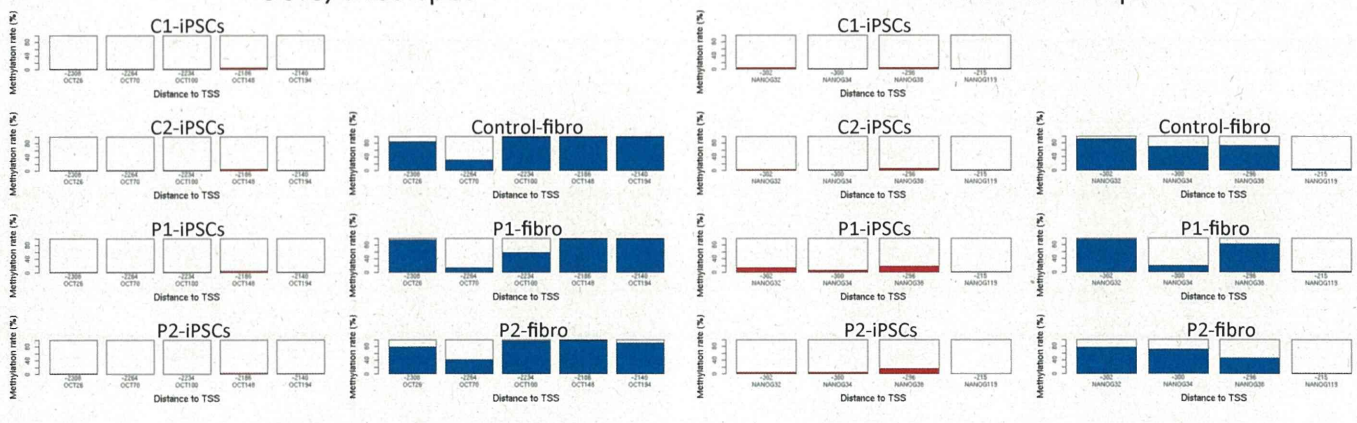
F
OCT3/4 TSS CpGs
NANOG TSS CpGs
C1-iPSCs
C2-iPSCs
P1-iPSCs
P2-iPSCs
Control-fibro
P1-fibro
P2-fibro
Methylation rate (%)
Distance to TSS

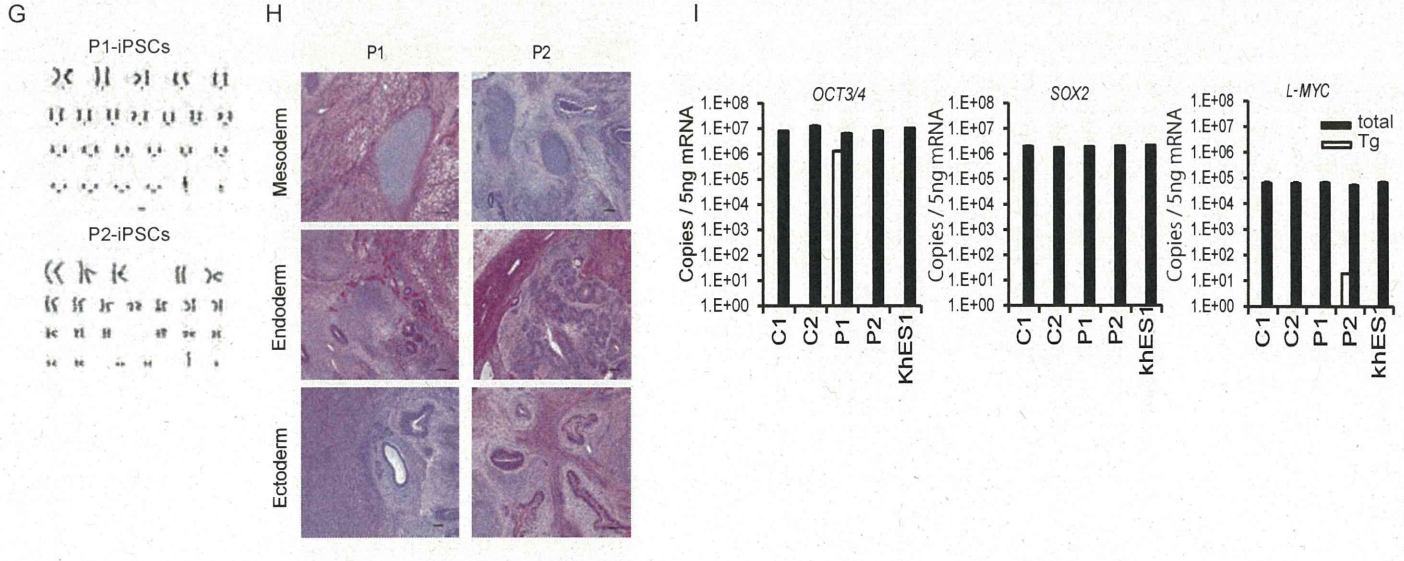
G
P1-iPSCs
P2-iPSCs
H
P1
P2
Mesoderm
Endoderm
Ectoderm
I
OCT3/4
SOX2
L-MYC
Copies / 5ng mRNA
total
Tg
C1
C2
P1
P2
KhES1

Figure S2

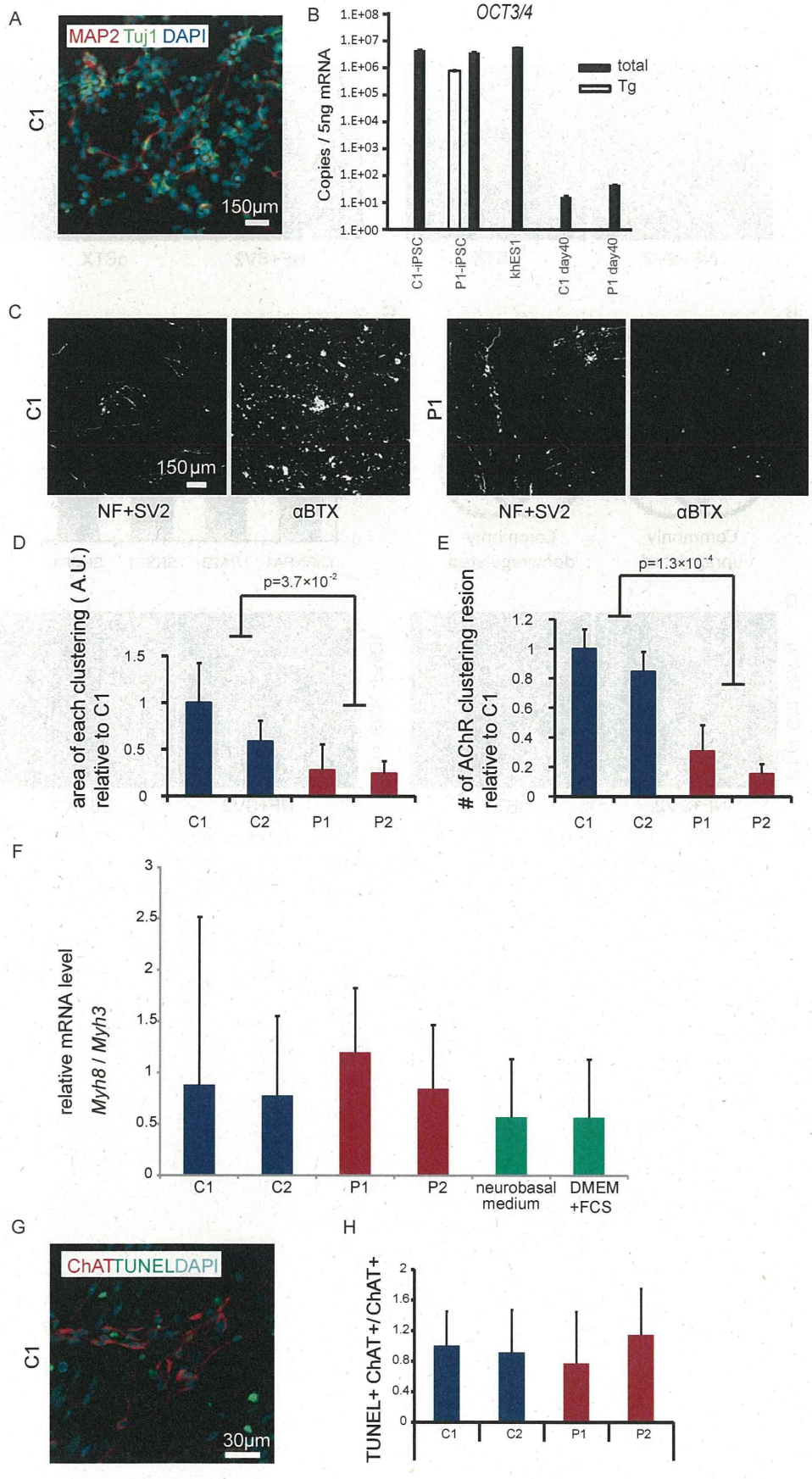
A
MAP2 Tuj1 DAPI
C1
150μm
B
OCT3/4
Copies / 5ng mRNA
1.E+08
1.E+07
1.E+06
1.E+05
1.E+04
1.E+03
1.E+02
1.E+01
1.E+00
total
Tg
C1-iPSC
P1-iPSC
khES1
C1 day40
P1 day40
C
C1
150μm
NF+SV2
αBTX
P1
NF+SV2
αBTX
D
area of each clustering (A.U.) relative to C1
p=3.7×10-2
1.5
1
0.5
0
C1
C2
P1
P2
E
# of AChR clustering resion relative to C1
p=1.3×10-4
1.2
1
0.8
0.6
0.4
0.2
0
C1
C2
P1
P2
F
relative mRNA level
Myh8 / Myh3
3
2.5
2
1.5
1
0.5
0
C1
C2
P1
P2
neurobasal medium
DMEM +FCS
G
ChATTUNELDAPI
C1
30μm
H
TUNEL+ ChAT+/ ChAT+
2
1.6
1.2
0.8
0.4
0
C1
C2
P1
P2

Figure S3

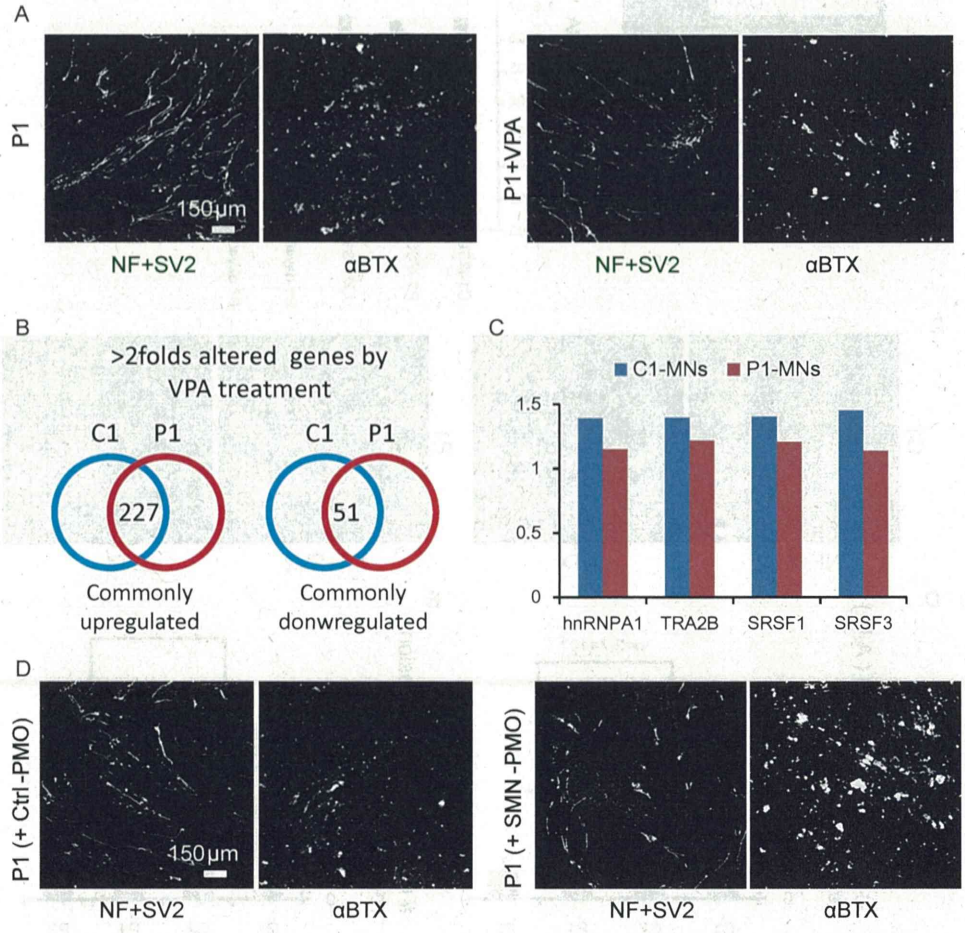
A
P1
150μm
NF+SV2
αBTX
P1+VPA
NF+SV2
αBTX
B
>2folds altered genes by VPA treatment
C1
P1
227
Commonly upregulated
C1
P1
51
Commonly donwregulated
C
C1-MNs
P1-MNs
1.5
1
0.5
0
hnRNPA1
TRA2B
SRSF1
SRSF3
D
P1 (+ Ctrl -PMO)
150μm
NF+SV2
αBTX
P1 (+ SMN -PMO)
NF+SV2
αBTX

Supplementary figure legends

Figure S1: Generation and characterization of SMA patient-specific iPSCs, related to Figure 1.
(A) Phase contrast images of SMA-iPSCs (P1, P2) showing typical pluripotent stem cell colony morphology. The immunocytochemical analysis revealed the expression of embryonic stem cell surface markers, SSEA-4, TRA-1-81. **(B)** The *NANOG* expression normalized to the *GAPDH* expression in control (C1, C2) and SMA-iPSCs (P1, P2) relative to hESCs (KhES1). Data are the means ±SEM of triplicate samples. **(C-E)** Microarray analysis of iPS clones. Control-fibroblasts are commercially available fibroblasts from a healthy volunteer. (C) Hierarchical clustering and (D) principal component analysis of iPSCs and parental fibroblasts. (E) Heatmap of gene sets preferentially expressed in pluripotent stem cells. **(F)** Methylation analysis of *OCT3/4* and *NANOG* promotor regions. Color boxes indicate methylated while white boxes indicate demethylated allele. **(G)** Karyotype analysis of iPSCs. **(H)** Teratoma formation assay showing successful differentiation of iPSCs into three germ layers. **(I)** The results of the quantitative RT-PCR analyses of *OCT3/4*, *SOX2* and *L-MYC* expression in control and SMA-iPSCs relative to hESCs (KhES1). "Tg" indicates primers detecting the transgene only, whereas "total" indicates primers detecting both the endogenous gene and the transgene. Scale bars: 100 μm. The data are the means ±SEM of triplicate samples.

Figure S2: Characteristics of iPSC-derived MNs and AChR clusters, related to Figure 2
(A) Immunostaining of SMA-iPSC-derived MNs. MAP2 (red) and Tuj1 (green) stained on day 40. **(B)** Quantitative RT-PCR analysis of the *OCT3/4* expression in the PSCs and PSC-derived MNs. The data are presented as the mean ±SEM of triplicate samples. **(C)** Processed black and white images used for automatic area counting of neurons and AChR clustering. NF+SV2 indicates neuron-positive areas and αBTX indicates AChR-clustering positive areas. **(D)** Quantitative analysis of the size of each AChR cluster. (means ±SEM, n=3, Wilcoxon rank-sum test). **(E)** Quantitative analysis of the number of AChR clusters. (means ±SEM, n=3, Wilcoxon rank-sum test). **(F)** Quantitative RT-PCR analysis of the expression of *Myh8* and *Myh3* genes in differentiated C2C12 myotubes. The ratio of *Myh8* to *Myh3* is shown. The data are presented as the mean ±SEM of triplicate dishes. Neurobasal medium; monocultured C2C12 cells were with co-culturing medium. DMEM+FCS; monocultured C2C12 cells with their maintenance medium. **(G)** The representative immunostaining image of iPSC-derived MNs with TUNEL (green) and ChAT (red) and **(H)** their quantification. The data are presented as the mean ±SEM of triplicate dishes.

Figure S3: Effect of VPA and PMO treatment on AChR clustering, related to Figure 3 and Figure 4.
(A) Processed black and white images used for automatic area counting of neurons and AChR clustering with or without VPA treatment. **(B)** Summary of RNA-seq analysis. **(C)** Expression levels of splicing factors (*SF2/ASF, Htra2-β1, SRp20, hnRNPA1*) with VPA treatment. Fold change to the expression levels without VPA treatment are shown. **(D)** Processed black and white images used for automatic area counting of neurons and AChR clustering after PMO treatment.

Table S1: list of genes upregulated by VPA treatment (>2 fold to compared to untreated), related to Figure 3.

TRIM34+TRIM6+TRIM6-TRIM34	CALCB	ARNTL
TMC6+TMC8	FGFR4	PPIC
ALS2CL	NCEH1	GSN
ETHE1	TMEM176B	SEMA3C
BLVRB	MITF	WNT16
FLJ46906	PIK3R5	EPOR
PPFIBP2	PPP1R1B	MFAP2
PTPN3	CACNA1G	SMYD3
NRGN	RTBDN	MUM1L1
PAQR5	RIT2	TAC3
AMBN	AKR1C3	TMEM255A
DUX2+DUX4+DUX4L2+DUX4L3+ DUX4L5+DUX4L6+DUX4L7	CXorf57	STEAP1
PAMR1	PENK	CRABP2
FSTL5	EGFL7	DENND2C
HOXD8	PLEKHB1	CAV2
DLEU1	GPR50	THEMIS2
CCDC152+SEPP1	NMNAT3	ALPL
CPT1A	ITM2A	TMCC3
MT2A	GLYATL1	GXYLT2
TMEM74	DPYD+DPYD-AS1	HLA-B
HLA-C	GABRE	ATP8B3
PRSS12	RAB7L1	LGALS1
CREG1	HLA-F+HLA-F-AS1	DNAJC12
SLC35F2	KCNJ4	IFI6
FXYD1	HEPH	IGSF1
DHRS2	ABCB1	CDK18
C4orf32	LRAT	TRAM1L1
NPAS1	VAV3	MIR1324
IL17RA	GPR158+GPR158-AS1	UTS2
PLCL1	SNORD114-8	GPC5
PLCG2	SERPINI1	PLEKHH2
DAPL1	CHRM4	IRF6
LPA	KCNIP2+LOC100289509	DPP10
NMRK1	CHRDL1	SULT1C4
TSPAN33	C9orf135	STAT4
USH2A	TESC	PAIP2B
IL16+STARD5	PRKCB	ARHGAP18
PPAP2C	KCTD19+PLEKHG4	C19orf77
TNNT1	TMEM176A	PRKCQ
ENPP5	GABRD	PPM1J
RASGRP2	CRYM	LPCAT2
SNORD61	HOXB7	PRKCG
HAPLN4	PDGFRA	C1orf115
FBLN2	ADRA1A	GRAMD1C
ARHGAP26	HPCA+TMEM54	TFEB
COL6A2	HERC5	ULBP1
DUSP23	KCNH3	ANO5
CHRNB4	OSTF1	TEX15
HLA-DPA1+HLA-DPB1	RAB11FIP1	GALNT10
SPAG6	MT1F	MIR5586
C3orf52	TPD52L1	RXRG
CYP2J2	SLC17A7	CD163L1
GALP	GMPR	C1QTNF9B+C1QTNF9B-AS1
STEAP1B	C4orf33	SLC2A4
SELL	CRLF1	TINCR
CRHR2	SNORA74A	LOC650368
CLDN6	TSPAN15	ALDH1A1
TMPRSS15	SCPEP1	SUSD3
IL13RA2	EDA	MIR3193
CD40	CLGN	C17orf96
RGS10	H2AFJ	DGAT2
MIR548AQ+MIR548AR	CD74	STAC2
C1QL1	MRAP2	SLC18A3
ITGA5	SYNPR	MIR7-3HG
GPX3	MIR4324	RNF128
NDST4	PLA2G4A	RLN2
PCBP3	ABCD2	FAM19A4
HLA-DMB	FTCD	RBM11
COL9A2	IFI30	C10orf128
TNNI3	A4GALT	LOC100506013
MICB	SLC9A9	RASD2
LOC401074	ARID5A	FAM101B
LOC401074	IMPA2	NRTN
MIR4735	MGARP	CHST9
SCGN	GPR37	ANKRD20A19P
ITIH5	SPINK2	

Table S2: list of genes downregulated by VPA treatment (>2 fold to compared to untreated), related to Figure 3.

EFCAB2	HYI+SZT2	MYD88
LINC00261	C4A+C4B+LOC100293534	LRFN4
TM4SF1	OBSL1	CLEC18A
BGLAP+PMF1+PMF1-BGLAP	GDPD2	SNORD4B
SNORD38B	ATP1A2	SNORD21
LPL	MIR93	MIR568
SNORD115-11+SNORD115-29+SNORD115-36+SNORD115-43	SERPINH1	ACSS1
LANCL2	SLC27A3	SNORD88A
AIFM2+H2AFY2	C4A+C4B+LOC100293534	SNORD12C
GLYCTK+MIR135A1	ACTG2	SOCS3
CLEC18C	MARVELD1	HIST1H2BC
MLC1	PDGFRB	MIR219-2+MIR2964A
SNORA51	RCBTB2	FADS2
MOV10	MIRLET7D	TAGLN
GTF2IRD2	MIR4508	MIR1305
MIR3175	MIR106B	CLEC18B
GTF2IRD2P1	SLC16A14	GTF2IRD2B